



# Monte Carlo simulations of zero electric field gradient liquid crystal mixtures

E. Elliott Burnell<sup>b,\*</sup>, Roberto Berardi<sup>a</sup>, Raymond T. Syvitski<sup>b</sup>, Claudio Zannoni<sup>a</sup>

<sup>a</sup> *Dipartimento di Chimica Fisica e Inorganica, Facoltà di Chimica Industriale, Università, Viale Risorgimento 4, I-40136 Bologna, Italy*

<sup>b</sup> *Department of Chemistry, University of British Columbia, 2036 Main Mall, Vancouver, BC, Canada V6T 1Z1*

Received 16 August 2000

## Abstract

We explore with Monte Carlo simulations the NMR finding that solutes in special nematic liquid crystal mixtures ‘feel’ zero average electric field gradient  $F_{ZZ}$ . The simulations involve solute–solvent mixtures of 1000 identical Gay–Berne ellipsoidal particles with added electric quadrupoles of varying strengths placed at particle centres. As long as all quadrupoles are sufficiently small,  $F_{ZZ}$  calculated at the particle centres is equal for all particles. For larger quadrupole moments, interactions among quadrupoles alter the interparticle distribution and subsequently  $F_{ZZ}$  depends on both solvent and solute quadrupoles; in general, the quadrupolar interactions produce a negative contribution to energy. © 2000 Elsevier Science B.V. All rights reserved.

## 1. Introduction

There exists evidence that the molecular quadrupole of small solute molecules (such as molecular hydrogen, acetylene, benzene and hexafluorobenzene) plays an important role in their orientational ordering in nematic liquid crystalline solvents [1]. Estimates of the average electric field gradient,  $F_{ZZ}$ , experienced by  $D_2$  [2,3] have been determined from deuterium NMR. Experiments on larger methyl- and chloro-substituted benzenes indicate that these larger solutes experience an  $F_{ZZ}$  of the same sign but reduced magnitude compared to that observed for  $D_2$  [4–6]. It is possible to prepare mixtures of liquid crystals for which the average  $F_{ZZ}$  experienced by small solutes is zero [7].

We refer to such mixtures as ‘magic mixtures’. While there is dispute in the literature on the relative importance of quadrupoles compared to that of other electrostatic interactions, there is good reason to describe the magic mixtures as ones for which only the size- and shape-dependent short-range interactions play a role. Evidence for this is given by the results of hard-body Monte Carlo (MC) simulations of ellipsoidal solutes in a system of ellipsoidal liquid crystal particles. The MC results are most closely accounted for by the same phenomenological model that best rationalizes NMR experiments on a collection of 46 solutes in a ‘magic mixture’ liquid crystal solvent [8,9].

MC simulations of hard-body 5:1 prolate ellipsoids containing a centred point quadrupole and one solute whose dimensions and quadrupole were varied have been reported [10]. The system was investigated for several values of solute and solvent quadrupoles. However, it was not possible

\* Corresponding author.

E-mail address: [elliott.burnell@ubc.ca](mailto:elliott.burnell@ubc.ca) (E.E. Burnell).

to reproduce the details of some NMR experiments, such as those on molecular hydrogen and acetylene, where the anisotropic interactions involving the molecular quadrupole yield an opposite sign of solute order parameter in the liquid crystals *N*-(*p*-ethoxybenzylidene)-*p'*-*n*-butylaniline (EBBA) and Merck ZLI 1132. In the simulations, the presence of a solute quadrupole tends to increase the solute orientational order for both signs of solvent quadrupole, and the field gradient observed at a particle centre was found to be a function of the quadrupoles of both solvent and solute.

In order to investigate this difference between NMR experiments and MC simulations, we choose here for study a set of Gay–Berne (GB) particles that are identical except for their quadrupoles. The GB potential incorporates both attractive and repulsive terms, and is thus considered more realistic than a hard-body potential. The aim is to understand the role played by molecular quadrupoles in liquid crystalline systems. In this investigation all particles are characterized by equal GB parameters; they differ only in the sign and magnitude of the quadrupole which is placed at the particle centre.

## 2. Details of the simulations

Monte Carlo simulations are performed on a total of 1000 GB 3:1 particles. In most cases the ‘solvent’ comprises  $N_S$  particles containing centred quadrupoles with major component  $Q_S^*$  and  $N_{S'} = 970 - N_S$  particles with  $Q_{S'}^* = -Q_S^*$ . The \* indicates a dimensionless variable that is defined in the footnote to Table 1. The solvent is described in terms of the mole fraction of S particles:  $X_S = 10^{-3} \times N_S$  for our simulations on 1000 particles. The additional 30 particles constitute the solutes, divided into three groups (*o*, *p* and *q*) of 10 particles each; two groups *p* and *q* have centred quadrupoles of value  $+Q_p^*$  and  $Q_q^* = -Q_p^*$ , while the third group has no quadrupole,  $Q_o^* = 0$ . Unless indicated otherwise, the concentration of each solute is  $X_o = X_p = X_q = 0.01$ .

The GB parameters used in this work for all particles are: the length-to-breadth ratio  $\kappa = 3$ ,

strength parameters  $\kappa' = 5$ ,  $\mu = 1$ , and  $\nu = 3$ , and the scaled number density  $\rho^* = 0.30$ . These parameters are chosen to ensure a fairly wide nematic range  $2.4 \leq T^* \leq 3.55$  [11]. The dimensionless temperature used here was  $T^* = 2.8$ , which is well within the nematic phase.

The initial MC configuration for all runs was a well-equilibrated GB configuration with  $Q^* = 0$ . The order parameter was 0.81. Unless otherwise indicated, 20 000 cycles were used for sample re-equilibration after the addition of quadrupoles, and averaging was performed over an additional 80 000 cycles. One long run (5 000 000 cycles using  $X_S = 0.500$  with  $Q_S^* = 1.0$ ,  $X_{S'} = 0.500$  with  $Q_{S'}^* = -Q_S^*$ , and  $X_o = X_p = X_q = 0$ ) was carried out to obtain sufficiently good statistics for the study of correlation functions.

## 3. Results and discussion

Contribution to the electric field gradient at the site of particle *i* due to the point quadrupole moment tensor  $Q_{\mu\nu}^{(j)}$  of particle *j* is [12]:

$$F_{\mu\nu}^{(ij)} = \frac{1}{r^5} \left[ -2Q_{\mu\nu}^{(j)} + 10Q_{\alpha\nu}^{(j)}\hat{r}_\alpha\hat{r}_\mu + 10Q_{\mu\alpha}^{(j)}\hat{r}_\alpha\hat{r}_\nu + 5Q_{\alpha\beta}^{(j)}\hat{r}_\alpha\hat{r}_\beta\delta_{\mu\nu} - 35Q_{\alpha\beta}^{(j)}\hat{r}_\alpha\hat{r}_\beta\hat{r}_\mu\hat{r}_\nu \right], \quad (1)$$

where  $\hat{r}$  is a unit vector describing the orientation of the displacement (*r*) between the quadrupole pair, and where we have used the Einstein summation convention for repeated indices. The quadrupolar contribution to the interparticle pair potential is a function of the electric field gradient due to particle *j* and the quadrupole tensor  $Q_{\mu\nu}^{(i)}$  of particle *i*:

$$U^{(Q^{(i)}Q^{(j)})} = -\frac{1}{3}Q_{\mu\nu}^{(i)}F_{\mu\nu}^{(ij)}. \quad (2)$$

The quadrupolar energy of the system,  $U^{(Q)}$ , is the sum of all such contributions, taking care not to count interactions twice [10].

The results of simulations with various solvent and solute quadrupoles are presented in Table 1, where we list the sample composition, the values of solvent and solute quadrupoles, the average field gradient,  $F_{ZZ,i}^*$ , observed at the centre of particle *i*, and the average contribution from quadrupole–



Table 1 (Continued)

| $X_S$ | $Q_S^*$ | $Q_p^*$ | $F_{ZZS}^*$ | $F_{ZZS'}^*$ | $F_{ZZo}^*$ | $F_{ZZp}^*$ | $F_{ZZd}^*$ | $F_{ZZa}^*$ | $F_{ZZb}^*$ | $U_S^{*(Q)}$ | $U_{S'}^{*(Q)}$ | $U_o^{*(Q)}$ | $U_q^{*(Q)}$ | $U_p^{*(Q)}$ |
|-------|---------|---------|-------------|--------------|-------------|-------------|-------------|-------------|-------------|--------------|-----------------|--------------|--------------|--------------|
| 0.960 | 1.0     | 0.5     | 0.507       | -0.960       | -0.144      | 0.191       | -0.543      | 0.191       | 0.191       | -0.132       | -0.293          | 0.000        | -0.087       | -0.020       |
| 0.960 | 1.0     | 1.0     | 0.504       | -1.015       | -0.175      | 0.506       | -1.014      | 0.506       | 0.506       | -0.132       | -0.303          | 0.000        | -0.302       | -0.131       |
| 0.960 | 1.0     | 2.0     | 0.546       | -1.080       | -0.201      | 1.188       | -2.200      | 1.188       | 1.188       | -0.143       | -0.319          | 0.000        | -1.270       | -0.651       |
| 0.960 | 2.0     | 0.2     | 3.444       | -6.353       | -0.083      | 0.373       | -0.494      | 0.373       | 0.373       | -1.901       | -3.663          | 0.000        | -0.036       | -0.013       |
| 0.960 | 2.0     | 0.5     | 3.411       | -6.307       | -0.103      | 0.914       | -1.317      | 0.914       | 0.914       | -1.891       | -3.657          | 0.000        | -0.207       | -0.116       |
| 0.960 | 2.0     | 1.0     | 3.432       | -6.420       | -0.098      | 1.864       | -2.680      | 1.864       | 1.864       | -1.901       | -3.714          | 0.000        | -0.819       | -0.502       |
| 0.960 | 2.0     | 2.0     | 3.471       | -6.326       | -0.118      | 3.491       | -6.542      | 3.491       | 3.491       | -1.930       | -3.653          | 0.000        | -3.757       | -1.937       |

<sup>a</sup>  $X_S$  is the mole fraction of particles with quadrupole  $Q_S^* = Q_S(\sigma_0^2/\epsilon_0)^{-1/2}$ .  $X_S' = 0.970 - X_S$  is the number of particles with quadrupole  $Q_S' = -Q_S^*$ . There are 10 particles each of solutes  $p$  (with quadrupole  $Q_p^*$ ),  $q$  (with quadrupole  $Q_q^* = -Q_p^*$ ), and  $o$  (with quadrupole  $Q_o^* = 0$ ). All particle  $i$  quadrupole tensors are traceless and axially symmetric with  $Q_i^*$  being the major tensor component corresponding to the particle's major axis. For the  $X_S = 0.500$  sample,  $X_S' = 0.500$  and there are no solutes.  $F_{ZZi}^* = F_{ZZi}(\sigma_0^2/\epsilon_0)^{1/2}$  is the ZZ tensor component of the average electric field gradient at particle  $i$ , and arises from the field gradients produced by quadrupoles on the surrounding particles.  $Z$  is the director direction.  $U_i^{*(Q)} = U_i^{(Q)}/\epsilon_0$  is the average energy arising from the quadrupole-quadrupole interactions of particle  $i$ . The parameter  $\epsilon_0$  is the strength parameter in the GB potential, and  $\sigma_0$  is the width of a 3:1 GB particle. Other dimensionless quantities are defined: distance  $r^* = r/\sigma_0$ ; temperature  $T^* = k_B T/\epsilon_0 = 2.8$ ; number density  $\rho^* = N\sigma_0^3/V = 0.3$ . Thus, for  $T = 280$  K and nematogen diameter  $\sigma_0 = 5$  Å (values appropriate for a typical nematic liquid crystal molecule),  $\epsilon_0 = 1.38 \times 10^{-14}$  erg.

quadrupole interactions to the energy of various particles. Values of  $Q^*$  are chosen to mimic those expected of real nematogens. Using the definitions in Table 1,  $Q^* = 1$  corresponds to  $Q \approx 6.6 \times 10^{-26}$  esu, a typical value for small solute molecules, and about 1/3 the value expected for a liquid crystal molecule such as EBBA;  $F_{ZZ}^* = 1$  corresponds to  $F_{ZZ} \approx 2.1 \times 10^{11}$  esu, a number comparable to those found by NMR in EBBA and ZLI 1132 [2–4,6].

Except for the sample with  $Q_S^* = 2$ , order parameters of all particles (with one exception), whether solute or solvent, were equal within statistical uncertainty in all simulations and were  $0.807 \pm 0.003$ . The one exception is the sample with  $Q_S^* = 1$  and  $Q_p^* = 2$  for which  $S_q = 0.819 \pm 0.006$  in all mixtures, and  $S_p = 0.815$  and  $0.819$  in the  $X_S = 0.740$  and  $X_S = 0.485$  samples. These slight increases in solute order parameters are barely significant. For the  $Q_S^* = 2$  samples, as shown in Table 2, all order parameters are slightly larger than 0.807 for all particles. In general, independent of the sign of  $Q^*$ , a larger  $Q^*$  is associated with a slightly larger particle order parameter. The most dramatic effect is for the  $Q_S^* = 2$ ,  $X_S = 0.485$  mixture where the order parameter increases to 0.88.

However, for this  $Q_S^* = 2$ ,  $X_S = 0.485$  mixture the correlation function  $g(z^*)$  shows a periodic density wave indicating that this mixture has formed a smectic phase. This is not surprising as the interaction between two precisely side-by-side quadrupoles of opposite sign is attractive, and would be expected to favour the formation of layers. It is interesting to note that a smectic phase has been observed for mixtures of liquid crystals whose components are nematic and for which the solute  $D_2$  experiences field gradients of opposite sign in the components [13]. In addition, because of the favourable interquadrupole interactions, a discotic phase results from simulations of oblate GB ellipsoids which contain quadrupoles of opposite sign [14]. The  $g(z^*)$  for the  $X_S = 0.960$  samples with small or zero quadrupoles show slight periodic density waves whose amplitude decreases as the magnitude of  $Q_S^*$  is increased. This is in agreement with a recent molecular dynamics study of GB particles (using different interaction

parameters than those used here, with all particles containing identical quadrupoles) where it was found that the presence of large quadrupoles tends to destabilize smectic phases and to stabilize nematic phases [15].

Effects of the different solvent and solute quadrupoles are conveniently observed in plots (Fig. 1) for constant solvent quadrupoles of the average field gradient observed at the various particle centres as a function of the value of solute quadrupole  $Q_p^*$  (where solute  $q$  has quadrupole  $Q_q^* = -Q_p^*$  and solute  $o$  has  $Q_o^* = 0$ ). In Fig. 1, a separate line is used for each solvent composition to plot the  $F_{ZZ}^*$  observed by each solute particle in the system. As the quadrupoles of solvent particles S and S' and of solute  $o$  ( $Q_o^* = 0$ ) are constant for each plot, it would be expected (as observed within the experimental error) that they give lines of zero slope. For clarity the lines for solvent S and S' particles are not shown.

NMR experiments have suggested that, in a given liquid crystal solvent, all solutes experience roughly the same  $F_{ZZ}$ . This is thought to be particularly true for the so-called magic mixtures for which  $F_{ZZ}$  (as 'felt' by  $D_2$ ) is zero. In this study all particles are described by the identical GB parameters, and can thus be thought of as having identical sizes and shapes. In analogy with the NMR experiments they would all be expected to 'feel' the same  $F_{ZZ}^*$ . In particular,  $F_{ZZ}^*$  is anticipated to be zero in the  $X_S = 0.485$  sample which has equal numbers of solvent quadrupoles of opposite signs: a zero value is found for  $F_{ZZ}^*$  for the  $Q_o^* = 0$  solute, as required by symmetry. Thus, this  $X_S = 0.485$  mixture is designed to mimic the magic mixture liquid crystal of the NMR experiments. However, a quick glance at Fig. 1 shows (in agreement with the simulations on hard 5:1 ellipsoidal systems [10], but in contradiction with the NMR results) that different solutes experience quite different  $F_{ZZ}^*$ 's, even in the  $X_S = 0.485$  sample.

Although the simulation results appear to contradict the NMR findings, we do note some interesting trends. First, when both liquid-crystal and solute quadrupoles are small, all solutes do experience roughly zero  $F_{ZZ}^*$  in the  $X_S = 0.485$  samples; and they also experience roughly the

same non-zero  $F_{ZZ}^*$  in the  $X_S = 0.740$  system (and a different non-zero  $F_{ZZ}^*$  in the  $X_S = 0.960$  system). This is most evident for  $Q_{\text{solute}}^* = 0.2$  in the graph for  $Q_S^* = 0.2$ . This observation is consistent with the trends observed in NMR experiments which have been interpreted in terms of all solutes experiencing the same  $F_{ZZ}$  which is taken to be a solvent property, and which is taken independent of the value of the solute quadrupole moment [1]. As the  $Q_S^*$  is increased from 0.2 to 1.0, the  $F_{ZZ}^*$  at the centre of solutes with zero  $Q_o^*$  values varies linearly with  $Q_S^*$  in the  $X_S = 0.740$  and  $X_S = 0.960$  samples, and remains zero in the  $X_S = 0.485$  mixture. However, the actual change (with solvent and solute quadrupoles) in  $F_{ZZ}^*$  at solutes with non-zero quadrupoles is quite dramatic, and depends on the absolute value of the solvent quadrupole and on both the sign and magnitude of the solute quadrupole.

Secondly, an examination of the sets of lines corresponding to  $X_S = 0.960$ ,  $X_S = 0.740$ , and  $X_S = 0.485$  for a given solute  $Q_p^*$  shows that the  $F_{ZZ}^*$  at the solute changes in a manner that is consistent with the NMR experiments, i.e., the change in  $F_{ZZ}^*$  is proportional to the solvent  $Q_S^*$  for  $Q_S^* \leq 1$ . This result is independent of the sign and magnitude of the solute quadrupole  $Q_p^*$ . In other words, there is a clear prediction that the  $F_{ZZ}^*$  values should change with mixing liquid crystals in a manner that is independent of the sign and magnitude of the solute quadrupole. Such an effect is consistent with the observed change with liquid crystal of the experimental order parameters of solutes such as acetylene, benzene, hexafluorobenzene, methyl fluoride, and  $D_2$ ; however, it does not explain the negative order parameters observed for acetylene and  $D_2$  in EBBA.

The actual change (with solvent and solute quadrupoles) in Fig. 1 of  $F_{ZZ}^*$  at solutes with non-zero quadrupoles is a major effect that appears contradictory to the NMR results. It is clear that this major effect depends on both the solute and solvent quadrupoles. Note especially that when  $Q_{\text{solute}}^* \neq 0$ ,  $F_{ZZ}^*$  is not zero in most magic mixture simulations. One might say that the only real magic mixture is the left part of the  $Q_S^* = 0.2$  (upper-left) panel of Fig. 1, up to the point that the curves for a given  $X_S$  start to diverge.

Table 2  
Solvent and solute order parameters for samples with  $Q_S^* = 2^a$

| $X_S$ | $Q_S^*$ | $Q_p^*$ | $S_S$    | $S_{S'}$  | $S_o$     | $S_q$     | $S_p$    |
|-------|---------|---------|----------|-----------|-----------|-----------|----------|
| 0.960 | 2.0     | 0.2     | 0.831(4) | 0.840(11) | 0.813(6)  | 0.815(7)  | 0.814(7) |
| 0.960 | 2.0     | 0.5     | 0.826(8) | 0.831(12) | 0.810(11) | 0.814(5)  | 0.812(6) |
| 0.960 | 2.0     | 1.0     | 0.827(7) | 0.836(9)  | 0.809(10) | 0.817(7)  | 0.816(7) |
| 0.960 | 2.0     | 2.0     | 0.827(6) | 0.836(7)  | 0.812(9)  | 0.838(14) | 0.827(6) |
| 0.740 | 2.0     | 0.2     | 0.837(7) | 0.853(6)  | 0.823(9)  | 0.823(8)  | 0.822(8) |
| 0.740 | 2.0     | 0.5     | 0.835(7) | 0.851(9)  | 0.820(9)  | 0.822(10) | 0.819(8) |
| 0.740 | 2.0     | 1.0     | 0.834(5) | 0.850(5)  | 0.819(5)  | 0.829(5)  | 0.821(6) |
| 0.740 | 2.0     | 2.0     | 0.837(6) | 0.853(6)  | 0.823(10) | 0.851(6)  | 0.838(6) |
| 0.485 | 2.0     | 0.2     | 0.885(5) | 0.885(4)  | 0.863(9)  | 0.864(8)  | 0.863(8) |
| 0.485 | 2.0     | 0.5     | 0.882(3) | 0.882(3)  | 0.861(5)  | 0.860(7)  | 0.861(4) |
| 0.485 | 2.0     | 1.0     | 0.882(2) | 0.882(3)  | 0.860(4)  | 0.865(4)  | 0.866(3) |
| 0.485 | 2.0     | 2.0     | 0.883(3) | 0.882(3)  | 0.862(7)  | 0.882(4)  | 0.882(3) |

<sup>a</sup> Order parameters are averages of numbers obtained from eight different 10,000 cycle calculations. Numbers in parentheses are  $10^3 \times$  standard deviations of these averages, and thus are estimates of error in the least significant digits reported.

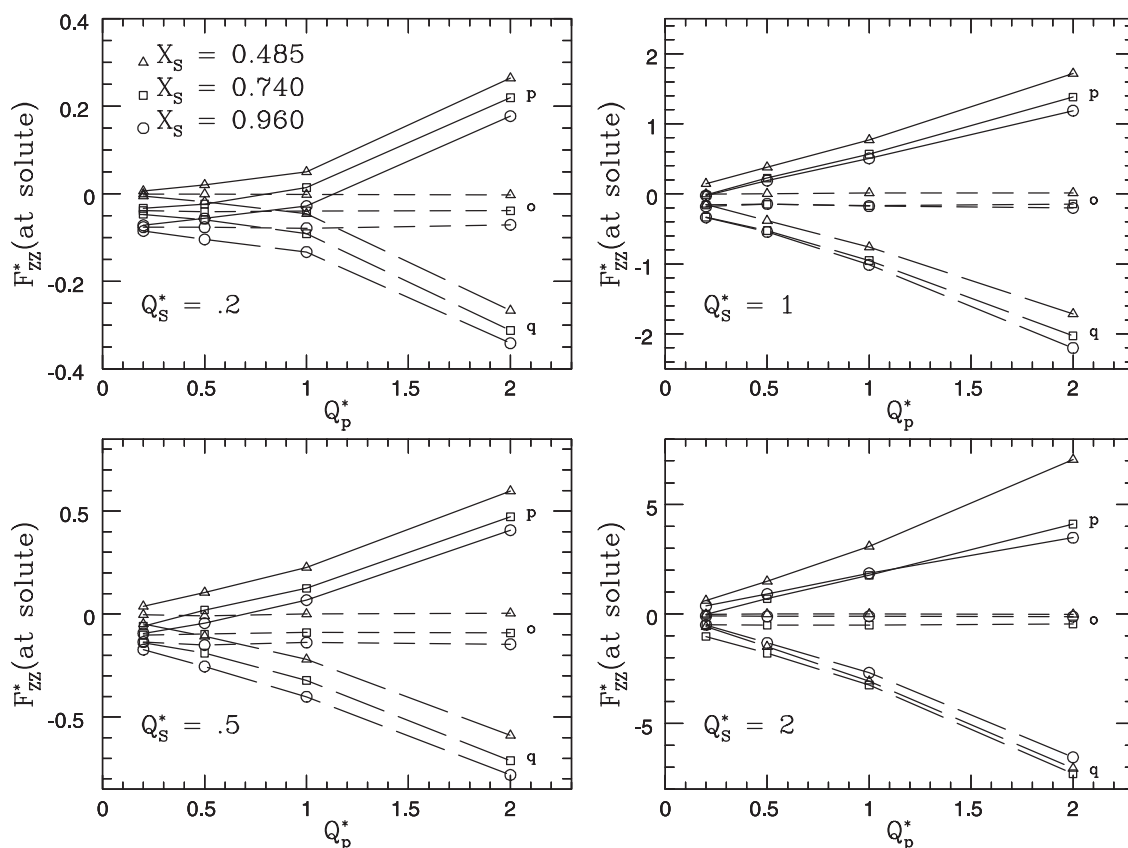


Fig. 1. Average electric field gradient at solute particle centre,  $F_{ZZ}^*$ , as a function of  $Q_p^*$ , the quadrupole moment for solute  $p$ . The results for solutes  $p$ ,  $q$  ( $Q_q^* = -Q_p^*$ ), and  $o$  ( $Q_o^* = 0$ ) are presented. The plots are labelled according to values for the positive solvent quadrupole components  $Q_S^* = 0.2, 0.5, 1.0$  and  $2.0$ . Note that the graphs have different vertical scales.

In order to examine the results in a different way, we present in Fig. 2 a plot of the  $F_{ZZ}^*$  at a solute divided by the absolute value of the solvent quadrupole,  $|Q_S^*|$ , versus the solute quadrupole (for clarity the  $X_S = 0.740$  results have been omitted). This representation of the results brings out some interesting features. For a given  $X_S$  value, the curves for  $Q_S^* = 0.2$  and  $Q_S^* = 0.5$  essentially overlap, and the curves for  $X_S = 0.960$  are a constant amount below those for  $X_S = 0.485$ . To be completely consistent with the NMR experiments, the curves should also be horizontal lines (the constant distance between the sets of curves is consistent, while the positive slope represents a disagreement). The deviations for larger  $X_S$  values are most likely associated with the restructuring of the solvent that eventually leads to the formation of a smectic phase in some cases. The deviation from the predicted horizontal line in  $F_{ZZ}^*(\text{at solute})/|Q_S^*|$  is generally larger than the difference associated with solvent composition. This graph shows dramatically the extent to which  $F_{ZZ}^*(\text{at solute})$

$/|Q_S^*|$  depends on the solute quadrupole, with the sign of  $F_{ZZ}^*(\text{at solute})$  usually being equal to the sign of the solute quadrupole. The positive slope is consistent with the energies given in Table 1, which are all either negative or very close to zero, independent of the signs of the quadrupoles involved. In other words, the effect of the quadrupole–quadrupole interaction is to modify in a subtle manner the local distribution of particles around a chosen particle such as to lower the quadrupole contribution to the total energy.

In order to understand these results, it is interesting to examine the effect that the interactions between point quadrupoles have on local structuring around the particles. An informative picture is obtained by examining pairwise correlation functions such as  $g_{SS'}(r^*)$  and  $g_{SS'}(z^*)$ , and the pairwise contribution to the quadrupolar energy,  $U_{SS'}^{*(Q)}$ , where  $z^* = z/\sigma_0$ . Such comparisons for the  $X_S = 0.500$ ,  $Q_S^* = 1.0$  system are presented in Fig. 3. The top-left panel presents  $g_{SS}(r^*)$ , the radial distribution of the like S solvent particles

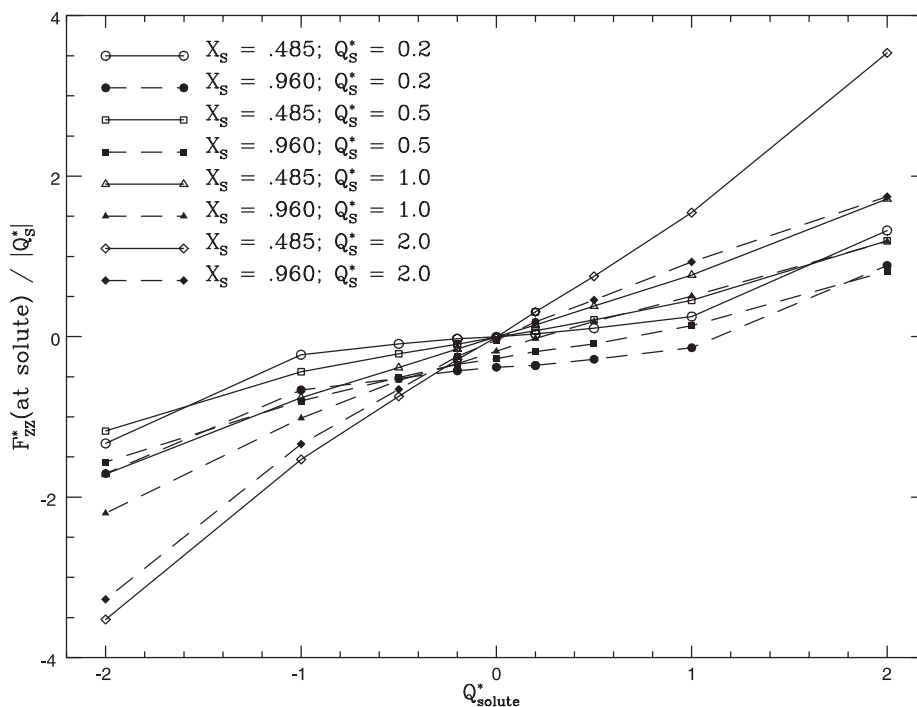


Fig. 2. Average electric field gradient at the solute particle centre divided by the absolute value of solvent quadrupole,  $|Q_S^*|$ , as a function of solute quadrupole. The values for solutes with quadrupole moments  $Q_p^*$ ,  $Q_q^* = -Q_p^*$ , and  $Q_o^* = 0$  are all included.

(dotted line shifted up by 0.4), and  $g_{SS'}(r^*)$ , the radial distribution of particles of type  $S'$  (negative quadrupole, solid line) around particles  $S$  (positive quadrupole, solid line). At first glance there appears to be almost no difference in the distribution of the like (SS) and unlike ( $SS'$ ) particles around a particle  $S$ . However, there are significant (albeit small) differences between the curves, and these are best observed by examining the difference  $g_{SS'}(r^*) - g_{SS}(r^*)$ , presented in the lower-left panel. It is clearly seen that particle  $S'$  has a preference for the smallest possible  $r^*$  value of 1.0 (one molecular diameter, unlike quadrupoles attract each other for a parallel side-by-side configuration), while particle  $S$  prefers a slightly larger  $r^*$  value (like

quadrupoles repel each other for a parallel side-by-side configuration). In this context, it is interesting to note that for very large like quadrupoles in this GB potential, particles tend to form dimers. For example, in a simulation using  $X_S = X_{S'} = 0.495$ , solvent quadrupole  $Q_S^* = 1.0$ , and 10 solute particles with quadrupole  $Q_p^* = 20$ , there are solute-solute dimers formed that are described with  $r^* = 0.9$ ,  $\theta_p = \theta_{p'} = 58^\circ$  and  $\theta_{pp'} = 22^\circ$  ( $\theta_p$  is the angle between the long axis of particle  $p$  and  $\hat{r}$ ;  $\theta_{pp'}$  is the interparticle dihedral angle). In this case particles with large quadrupoles have placed themselves in a negative energy configuration; the low value for  $r^*$  is indicative of the strength of the quadrupole interactions between such large

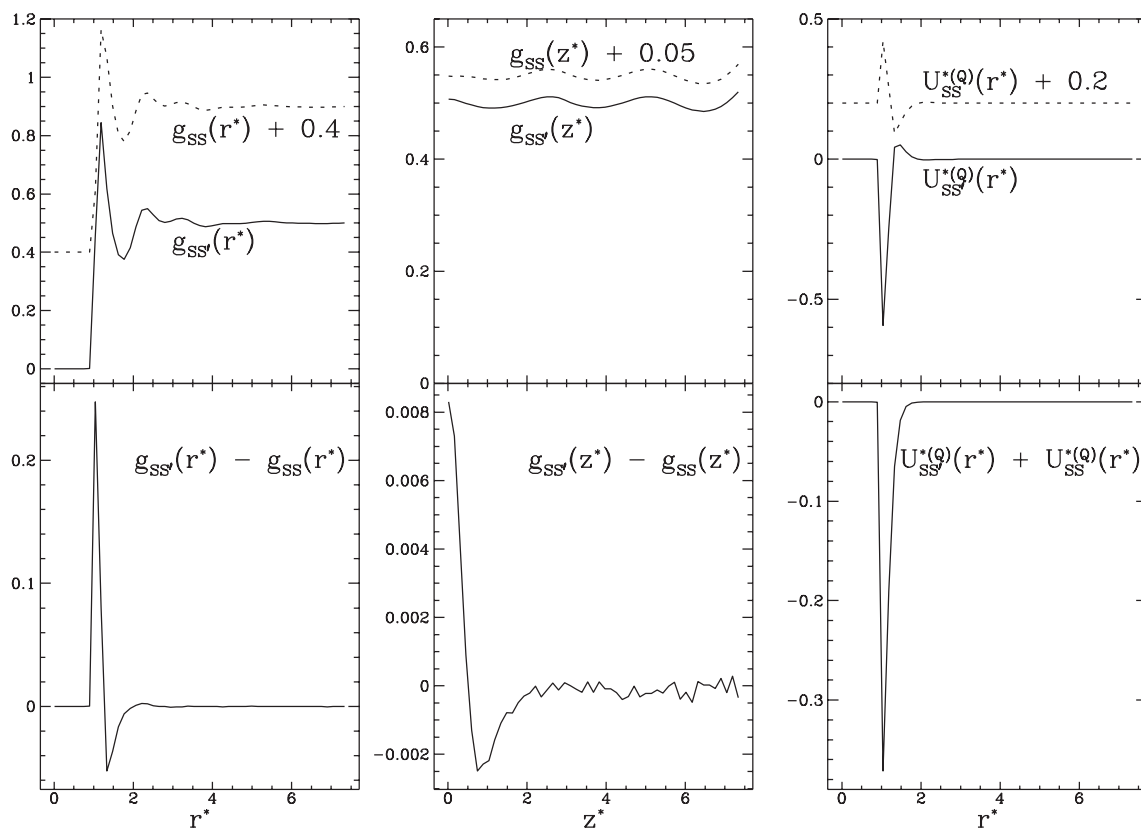


Fig. 3. Correlation functions ( $g_{ij}(r^*)$  and  $g_{ij}(z^*)$ ) and quadrupolar energies  $U_{ij}^{*(Q)}(r^*)$  for a simulation of a 500/500 mixture of particles with quadrupole moments +1 and -1. The graphs are an average over 5 000 000 cycles of the system. The upper graphs show the contributions to correlation functions and quadrupolar energies for  $ij = SS$  and  $ij = SS'$  interactions, while the lower graphs for the correlation functions are the difference between the two upper graphs, and for the quadrupolar energies are the sum of the two upper graphs. We estimate the error to be within  $10^{-3}$ . The SS graphs are offset for clarity.  $SS'$  functions are equivalent to SS functions.

quadrupoles. Angles for this configuration are probably similar to those associated with the favourable interactions between like quadrupoles in Fig. 3 where the lower quadrupole–quadrupole interaction energy leads to  $r^* > 1.0$ .

Graphs for the comparison of  $g_{SS}(z^*)$  and  $g_{SS'}(z^*)$  are presented in Fig. 3 (centre panels), and the preference for the like particles to slide a little along the  $z$  axis, while the unlike particles favour an adjacent alignment, is easily noted in the difference plot of the lower centre panel. The favourable energy configuration corresponding to the shift for like particles compared to unlike is noted in the radial energy distribution plots of the right panels of Fig. 3. The summed plot of the lower right panel emphasizes that the different signs associated with the energies of S–S and S–S' interactions tend to cancel the quadrupolar contribution to the energy at large  $r^*$ ; the negative dip at small  $r^*$  values emphasizes the attraction between unlike and the repulsion between like particles that leads to an excess of unlike pairs at small  $r^*$  values.

Effects of the structuring caused by the quadrupole interaction can perhaps be more effectively demonstrated in a two-dimensional plot of particle distribution as a function of both interparticle separation  $r^*$  and cosine of the angle between the interparticle axis and the director,  $\cos \beta_r$ , as presented in the difference plot Fig. 4 for the  $X_S = 0.500$ ,  $Q_S^* = 1.0$  simulation. The effect of interactions between quadrupoles is evident in the preference for SS' interactions at small  $r^*$  values with  $\beta_r \approx 90^\circ$ , and the preference for like interactions shown by the positive bump in the graph.

In this study we have examined 3:1 ellipsoidal GB particles, and have measured the  $F_{ZZ}^*$  at their centres. As found in the previous simulations, the presence of quadrupoles has essentially no effect on the order parameter of solutes of the same dimension as the liquid crystal; however, large quadrupoles do enhance orientational order. Magic mixtures can be simulated as long as both solvent and solute quadrupoles are kept sufficiently small. For larger quadrupoles, the simulations agree with the earlier ones that employ hard-body ellipsoids [10]. Interactions between

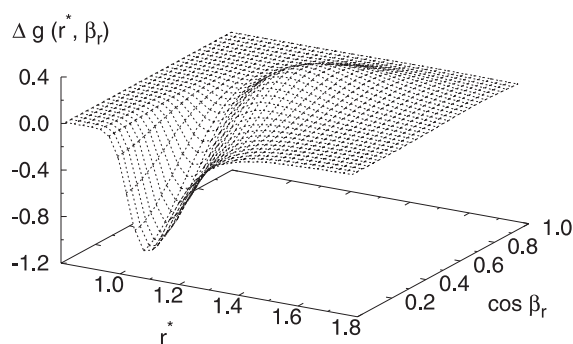


Fig. 4. The difference between the SS and SS' correlations,  $\Delta g(r^*, \beta_r)$ , as a function of  $r^*$  and  $\cos \beta_r$ , where  $\beta_r$  is the angle between the interparticle vector and the director.

particles that contain large quadrupoles lead to a rearrangement of the surrounding quadrupolar particles so as to lower the energy: this effect even applies to particles with the same sign of  $Q^*$ .

## Acknowledgements

We thank James Polson for stimulating discussions. EEB thanks his co-workers at the University of Bologna for their wonderful hospitality and scientific interactions during his sabbatical leave there in 1998, and is grateful to the Natural Science and Engineering Research Council of Canada for financial support. C.Z. and R.B. thank the University of Bologna, MURST *PRIN Cristalli Liquidi* and EU *TMR* contract FMRX-CT97-0121 for the financial support.

## References

- [1] E.E. Burnell, C.A. de Lange, *Chem. Rev.* 98 (1998) 2359.
- [2] G.N. Patey, E.E. Burnell, J.G. Snijders, C.A. de Lange, *Chem. Phys. Lett.* 99 (1983) 271.
- [3] A.J. van der Est, E.E. Burnell, J. Lounila, *J. Chem. Soc., Faraday Trans. 2* 84 (1988) 1095.
- [4] R.T. Syvitski, E.E. Burnell, *Chem. Phys. Lett.* 281 (1997) 199.
- [5] R.T. Syvitski, Ph.D. thesis, University of British Columbia, 2000.
- [6] R.T. Syvitski, E.E. Burnell, *J. Chem. Phys.* 113 (2000) 3452.
- [7] P.B. Barker, A.J. van der Est, E.E. Burnell, G.N. Patey, C.A. de Lange, J.G. Snijders, *Chem. Phys. Lett.* 107 (1984) 426.

- [8] J.M. Polson, E.E. Burnell, *Mol. Phys.* 88 (1996) 767.
- [9] R.T. Syvitski, J.M. Polson, E.E. Burnell, *Int. J. Modern Phys. C* 10 (1999) 403.
- [10] J.M. Polson, E.E. Burnell, *Phys. Rev. E* 55 (1997) 4321.
- [11] R. Berardi, A.P.J. Emerson, C. Zannoni, *J. Chem. Soc., Faraday Trans.* 89 (1993) 4069.
- [12] A.D. Buckingham, *Adv. Chem. Phys.* 12 (1967) 107.
- [13] J. Jokisaari, P. Diehl, O. Muenster, *Mol. Cryst. Liq. Cryst.* 188 (1990) 189.
- [14] M.A. Bates, G.R. Luckhurst, *Liq. Cryst.* 24 (1998) 229.
- [15] M.P. Neal, A.J. Parker, *Chem. Phys. Lett.* 294 (1998) 277.